Proceedings of the ASME 2014 Dynamic Systems and Control Conference
DSCC2014
October 22-24, 2014, San Antonio, TX, USA

OPTIMAL VEHICLE MOTION CONTROL TO MITIGATE SECONDARY CRASHES AFTER AN INITIAL IMPACT

Byung-joo Kim
Department of Mechanical Engineering
University of Michigan
Ann Arbor, MI, USA
Email: bjukim@umich.edu

Huei Peng
Department of Mechanical Engineering
University of Michigan
Ann Arbor, MI, USA
Email: hpeng@umich.edu

ABSTRACT

Typical drivers are not ready to react to unexpected collisions from other vehicles. The initial impact can startle the driver who then fails to maintain control. Since a loss of control leads to intense skidding and undesirable lateral motions, more severe subsequent events are likely to occur. To reduce the severity of possible subsequent (secondary) crashes, this paper considers both vehicle heading angle and lateral deviation from the original driving path. The research concept here is different from today's electronic stability control systems in that it activates the differential braking even when the magnitude of yaw rate or vehicle slip angle is very high. In addition, the lateral displacement and yaw angle with respect to the road are part of the control objective. The Linear Time Varying Model Predictive Control (LTV-MPC) method is used, with the key tire nonlinearities captured through linearization. We consider tire force constraints based on the combined-slip tire model and their dependence on vehicle motion. The computed high-level (virtual) control signals are realized through a control allocation problem which maps vehicle motion commands to tire braking forces considering constraints. Numerical simulation and analysis results are presented to demonstrate the effectiveness of the control algorithm.

INTRODUCTION

Approximately, 5.6 million motor vehicle crashes were reported in 2012 in the United States, resulting in about 33,500 fatalities [1]. Among them, over 30% of all crashes have two or more harmful events following the initial collision. Several statistical studies based on vehicle crash data [2-4] indicate that number of multiple impact crashes has been increasing. These reports found that the risk of severe injuries is much higher in multiple impact crashes than in single impact crashes. In [5], it is also pointed out that the risk of both injuries and fatalities increased with the number of collision events. Multiple impact crashes can be more dangerous because drivers are not prepared for impacts from the side or back, as the most drivers focus on the front view. Since looking ahead and using an inside rearview mirror cannot always provide enough information of adjacent lanes [6], the continuous monitoring of surroundings while maintaining a lane may not be an easy task for the average driver. For this reason, drivers can panic or fail to respond to an unexpected initial event, and thus lose control. When drivers react improperly, undesirable vehicle motions can lead to hazardous heading angles and excessive lateral deviation, resulting in harmful secondary crashes. One of the crash analysis reports in NHTSA (National Highway Traffic Safety Administration) [7] presents the vehicle spin angle distribution in the most harmful secondary event crashes. It shows that secondary events at around 90° turns, either clockwise or counter clockwise, cause the most harmful secondary crashes. As shown in [8], based on the injury scale level data, side impacts in a secondary event are more harmful to the occupants. Since the sides of a vehicle have less crash-energy absorbing structures than the frontal and rear sections, the risk of fatalities and serious injuries with side crashes is higher [9]. Moreover, an analysis investigating vehicle dynamic motion after an impact in [10] shows that an excessive lateral lane deviation after an initial impact plays a key role in the risk of secondary impacts.

Secondary crashes can be partly mitigated by employing a vehicle Electronic Stability Control (ESC). However, the effectiveness of ESC to mitigate secondary crashes has not been fully taken advantage of [11]. Since these control algorithms were designed to intervene after a vehicle-to-vehicle impact, only limited control actions can be applied. Some ESC could even turn off if the yaw rate or lateral acceleration is too high, because the situation can be misinterpreted as a sensor failure. Hence, a new feature must be designed to mitigate secondary crashes. To enhance ESC performance after an initial crash, several control concepts in the literature were devised using steering or braking [12-14]. Recently, a secondary

collision braking strategy has been available on production vehicles by the name of "Secondary Collision Brake Assist". EURO NCAP (New Car Assessment Program) believes that this system can reduce fatalities and serious injuries [15]. However, these systems are usually either limited to work after a mild collision scenario or did not consider hazardous heading final angle. Considering the fact that the sides of vehicles are more vulnerable than the front or rear, the vehicle heading angle is an important parameter that needs to be controlled for secondary collision safety. In addition, a small lateral deviation after an initial collision is desired to reduce the risk of secondary collision with roadside objects or vehicles in other lanes. The proposed control concept in this paper includes allowing a high yaw motion to avoid vulnerable heading angles (e.g. 90°, 270°). This paper focuses on a vehicle motion control strategy which leads a vehicle to a safe heading angle (0°, 180°, 360°, etc.) while maintaining small lateral displacement. The underlying assumption is that the sensors and actuators still function normally after the first impact. The heading angle and lateral speed are assumed to be available from a reliable vision, magnetometer, or GPS sensor [16]. And no driver steering action is considered in the current design.

VEHICLE MODEL AND TIRE MODEL

The vehicle model considers longitudinal, lateral, and yaw motions of the vehicle as shown in Fig. 1. The governing equations are:

$$\begin{aligned} m\dot{V}_X &= F_{x,f_{L+R}}\cdot\cos(\psi+\delta)+F_{x,r_{L+R}}\cdot\cos(\psi) \\ &\quad -F_{y,f_{L+R}}\cdot\sin(\psi+\delta)-F_{y,r_{L+R}}\cdot\sin(\psi) \end{aligned} \tag{1}$$

$$\begin{aligned} m\dot{V}_Y &= F_{x,f_{L+R}}\cdot\sin(\psi+\delta)+F_{x,r_{L+R}}\cdot\sin(\psi) \\ &\quad +F_{y,f_{L+R}}\cdot\cos(\psi+\delta)+F_{y,r_{L+R}}\cdot\cos(\psi) \end{aligned} \tag{2}$$

$$\begin{aligned} I_{zz}\dot{r} &= a\cdot\left(F_{x,f_{L+R}}\cdot\sin(\delta)+F_{y,f_{L+R}}\cdot\cos(\delta)\right) \\ &\quad -b\cdot F_{y,r_{L+R}}+(T_W/2)\cdot\left\{\left(F_{x,f_R}-F_{x,f_L}\right)\cdot\cos(\delta)\right\} \\ &\quad +(T_W/2)\cdot\left\{-\left(F_{y,f_R}-F_{y,f_L}\right)\cdot\sin(\delta)+\left(F_{x,r_R}-F_{x,r_L}\right)\right\} \end{aligned} \tag{3}$$

The longitudinal and lateral forces for each tire are denoted by $F_{x,\oplus_\odot}, F_{y,\oplus_\odot}$ which are defined in a tire fixed coordinate. The subscript ($\oplus\in\{f,r\}$) represents the front and rear axles and the next subscript denotes the left and right side of the vehicle ($\odot\in\{L,R,L+R\}$). x and y are axes of a coordinate system located at the center of gravity (CG) in the vehicle fixed frame, while X and Y indicate vehicle position in the inertial coordinate. The motion of the vehicle is defined by vehicle velocities V_X, V_Y associated with X and Y, the steering angle δ at the front tires, the heading angle ψ, and the yaw rate r. Vehicle geometries are represented by a, b, and T_W which are distances to front and rear axles from the CG location and the width of the vehicle. M is the vehicle mass and I_{zz} is the vehicle yaw moment of inertia. It should be noted that the equations are formed in inertial coordinate to explicitly consider the lateral displacement. Considering the fact that longitudinal brake forces of each tire are independent controls in differential braking, Eq. (1), (2), and (3) can be constructed as a six-state nonlinear first-order system:

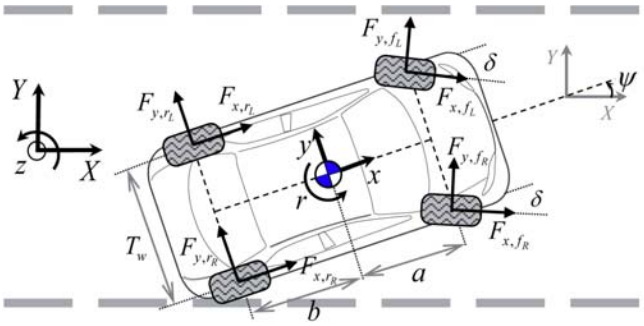

FIGURE 1. Vehicle motion with respect to a lane in the XY-plane

$$\dot{\xi}(t) = f(\xi,t)+g(\xi,u,t) \tag{4}$$

where, $\xi=\begin{bmatrix} X & V_X & Y & V_Y & \psi & r\end{bmatrix}$ and

$$f(\xi,t)=\begin{bmatrix} V_X \\ -\left\{F^0_{y,f_{L+R}}\sin(\psi+\delta)+F^0_{y,r_{L+R}}\sin(\psi)\right\}/M \\ V_Y \\ \left\{F^0_{y,f_{L+R}}\cos(\psi+\delta)+F^0_{y,r_{L+R}}\cos(\psi)\right\}/M \\ r \\ \begin{Bmatrix} a\cdot F^0_{y,f_{L+R}}\cos(\delta)-b\cdot F^0_{y,r_{L+R}}\sin(\delta) \\ -(T_W/2)\cdot\left(F^0_{y,f_R}-F^0_{y,f_L}\right)\sin(\delta)\end{Bmatrix}/I_{zz}\end{bmatrix} \tag{4a}$$

$$g(\xi,u,t)=\begin{bmatrix} 0 \\ \left\{F_{x,f_{L+R}}\cos(\psi+\delta)+F_{x,r_{L+R}}\cos(\psi)\right\}/M \\ 0 \\ \left\{F_{x,f_{L+R}}\sin(\psi+\delta)+F_{x,r_{L+R}}\sin(\psi)\right\}/M \\ 0 \\ \begin{Bmatrix} a\cdot F_{x,f_{L+R}}\sin(\delta)+\dfrac{T_W}{2}\left(F_{x,r_R}-F_{x,r_L}\right) \\ +(T_W/2)\cdot\left(F_{x,f_R}-F_{x,f_L}\right)\cos(\delta)\end{Bmatrix}/I_{zz}\end{bmatrix} \tag{4b}$$

$$+\begin{bmatrix} 0 \\ -\left\{\Delta F_{y,f_{L+R}}\sin(\psi+\delta)+\Delta F_{y,r_{L+R}}\sin(\psi)\right\}/M \\ 0 \\ \left\{\Delta F_{y,f_{L+R}}\cos(\psi+\delta)+\Delta F_{y,r_{L+R}}\cos(\psi)\right\}/M \\ 0 \\ \begin{Bmatrix} a\cdot\Delta F_{y,f_{L+R}}\cos(\delta)-b\cdot\Delta F_{y,r_{L+R}} \\ -(T_W/2)\cdot\left(\Delta F_{y,f_R}-\Delta F_{y,f_L}\right)\sin(\delta)\end{Bmatrix}/I_{zz}\end{bmatrix}$$

Here, u represents the independent 4-wheel brake control actions ($u = \begin{bmatrix} F_{x,f_L} & F_{x,f_R} & F_{x,r_L} & F_{x,r_R} \end{bmatrix}$), $F^0_{y,\oplus_\circlearrowright}$ are the lateral tire forces at a known slip angle under zero longitudinal slip condition, and $\Delta F_{y,\oplus_\circlearrowright}$ are the induced lateral tire force ($\Delta F_{y,\oplus_\circlearrowright} = F_{y,\oplus_\circlearrowright} - F^0_{y,\oplus_\circlearrowright}$) caused by the combined-slip effect. It should be noted that $f(\xi,t)$ is not related to the control inputs (u), while $g(\xi,u,t)$ is split into two parts: the direct effect of control inputs ($F_{x,\oplus_\circlearrowright}$), and indirect effect (disturbance) due to induced lateral force ($\Delta F_{y,\oplus_\circlearrowright}$). Later, we will solve the control problem in two steps: first, solve the virtual control input $g(\xi,u,t)$, and then compute the tire force $F_{x,\oplus_\circlearrowright}$ that will track the virtual control input, despite of the combined-slip tire nonlinearities.

For an effective vehicle control action, accurate tire force characterization is important. We use Pacejka's Magic Formula tire model [17], which describes combined longitudinal and lateral forces as functions of the tire slip angles (α), the slip ratio (λ), and vertical loads (F_z):

$$\begin{bmatrix} F_{x,tire} & F_{y,tire} \end{bmatrix}^T = P\left(\frac{C_\alpha \|s\|}{F_p(F_z)}, C, E \right) \cdot \frac{F_p(F_z)}{\|s\|} \cdot s \tag{5}$$

where, $s = \begin{bmatrix} s_x & s_y \end{bmatrix}^T = \begin{bmatrix} \lambda & \tan\alpha \end{bmatrix}^T$ (5a)

$$P(\chi, C, E) = \sin\left[C \cdot \arctan\left\{ \frac{\chi}{C} - E\left(\frac{\chi}{C} - \arctan\left(\frac{\chi}{C} \right) \right) \right\} \right] \tag{5b}$$

$$F_p(F_z) = F_z \Big/ \left(1 + \left(1.5 \cdot \frac{F_z}{M \cdot g} \right)^3 \right) \tag{5c}$$

$$C_\alpha = c_1 \cdot M \cdot g \cdot \left(1 - e^{-\frac{c_2 \cdot F_z}{M \cdot g}} \right) \tag{5d}$$

In this function, road friction coefficient (μ) is assumed to be fixed on a dry asphalt ($\mu = 0.85$). The tire slip angles are:

$$\alpha_{f_L} = -\delta + \arctan \frac{v_{y,f_L} + a \cdot r}{v_{x,f_L} - (T_W / 2) \cdot r} \tag{6}$$

$$\alpha_{f_R} = -\delta + \arctan \frac{v_{y,f_R} + a \cdot r}{v_{x,f_R} + (T_W / 2) \cdot r} \tag{7}$$

$$\alpha_{r_L} = \arctan \frac{v_{y,r_L} - b \cdot r}{v_{x,r_L} - (T_W / 2) \cdot r} \tag{8}$$

$$\alpha_{r_R} = \arctan \frac{v_{y,r_R} - b \cdot r}{v_{x,r_R} + (T_W / 2) \cdot r} \tag{9}$$

The tire force profiles over the entire range of tire slip angle and longitudinal slip ratio are shown in Fig. 2. When α is near 0 or ±180°, both longitudinal and lateral forces vary significantly with λ. On the contrary, the effects of λ are small when α is around ±90°, meaning that braking action is not effective.

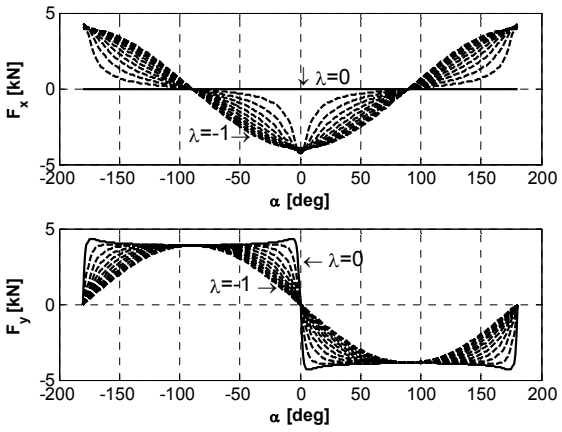

FIGURE 2. Longitudinal and lateral forces as functions of the tire slip angle and longitudinal slip ratio (-1≤λ≤0)

ANAYSIS OF EFFECTIVE TIRE FORCE RANGES

Because of the coupling effect of longitudinal-lateral forces, the induced lateral tire force (ΔF_y) generated by the tire brake force (F_x), needs to be considered to compute the vehicle lateral and yaw motions. Equation (10)-(13) show the vehicle yaw moments ($M_{z,\oplus_\circlearrowright}$) calculated by the moment arm from the CG point to the forces $F_{x,\oplus_\circlearrowright}$ and $\Delta F_{y,\oplus_\circlearrowright}$.

$$\begin{aligned} M_{z,f_L} = {} & F_{x,f_L} \cdot \left(a \cdot \sin(\delta) - (T_W / 2) \cdot \cos(\delta) \right) \\ & + \Delta F_{y,f_L} \cdot \left(a \cdot \cos(\delta) + (T_W / 2) \cdot \sin(\delta) \right) \end{aligned} \tag{10}$$

$$\begin{aligned} M_{z,f_R} = {} & F_{x,f_R} \cdot \left(a \cdot \sin(\delta) + (T_W / 2) \cdot \cos(\delta) \right) \\ & + \Delta F_{y,f_R} \cdot \left(a \cdot \cos(\delta) - (T_W / 2) \cdot \sin(\delta) \right) \end{aligned} \tag{11}$$

$$M_{z,r_L} = -F_{x,r_L} \cdot (T_W / 2) - \Delta F_{y,r_L} \cdot b \tag{12}$$

$$M_{z,r_R} = F_{x,r_R} \cdot (T_W / 2) - \Delta F_{y,r_R} \cdot b \tag{13}$$

From these kinematic relationships, possible ranges of yaw moment acting on a vehicle CG point can be obtained with various wheel slip ratios from free rolling (λ=0) to fully locked (λ=-1). As shown in Fig. 3, it is noted that the most effective wheel to change yaw moment can be determined based on the vehicle side slip angle. For example, there might be a case when the vehicle needs a positive yaw moment and the slip angles of all tires are small positive. In this case, the front-left wheel is the best candidate because the yaw moment on that tire (M_{z,f_L}) shows a greater positive value than others. Similarly, right rear wheel is the best to use for negative yaw moment generation under the same situation. It should be noted that there exist regions that have almost no control authorities for yaw moment control. In Fig. 3, it can be seen that when the tire slip angle is around ±90 degrees, little yaw moment can be generated. i.e., it is hard to control vehicle yaw motion in those situations. Examples above indicate the importance of understanding vehicle dynamics, especially tire saturation

constraints, when designing a controller such as the model predictive control method to be used in this paper. Although we only presented the vehicle yaw motion results, one also should find other feasible control regions for longitudinal or lateral vehicle motions. In those cases, the vehicle heading angle needs to be considered together with the tire slip angle and slip ratio.

LINEAR TIME VARYING MODEL PREDICTIVE CONTROL

The first step to implement the model predictive control (MPC) is the linearization of the nonlinear vehicle dynamics about every operating point so that a quadratic programming structure can be applied [18, 19]. This method decomposes the nonlinear design problem into several linear sub-problems. The successive linearization points do not need to be equilibriums. MPC finds a cost-minimizing control sequence over the prediction horizon. At the same time, it incorporates feasible control bounds so that control signals are implementable–critical for the MPC to work satisfactorily. Moreover, the MPC is applicable to real-time processing because of the low computation requirement of the linear time-varying MPC (LTV-MPV).

Architecture of the Proposed Control System

The overall control structure is shown in Fig. 4. The desired vehicle states are first compared with their current states. Then, in response to the state errors, the LTV-MPC controller determines the desired virtual controls based on the QP (Quadratic Programming) optimization solution under feasible vehicle dynamic constraints. Coupling between the tire longitudinal and lateral forces is considered in figuring out the control constraints. Next, the optimal control allocation process maps the virtual control demand onto individual wheel brake forces. In the last stage, actuator controllers manipulate physical variables, such as wheel cylinder braking pressures, to achieve the desired tire forces. Then, this actuator action affects vehicle motion and the resulting vehicle states are measured or estimated for the feedback control.

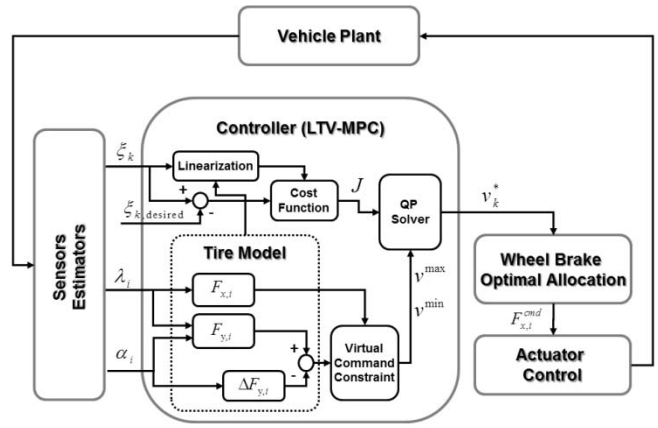

FIGURE 4. Architecture of the proposed control system

Linearizing at Non-Equilibrium Points

Considering the nonlinear dynamics shown in Eq. (4), the linearization is done through Taylor expansion around points (ξ_0), and virtual control input (v) is introduced from the simple relationship ($g(\xi,u,t)=B_v\cdot v$):

$$\begin{aligned}&\dot{\xi}(t)\approx f(\xi_0,t)+A(t)\cdot(\xi-\xi_0)+B_v\cdot v(t)\\&\Rightarrow\dot{\xi}(t)=A(t)\cdot\xi+B_v\cdot v(t)+B_\tau\cdot\tau(t)\end{aligned}\tag{14}$$

$$\text{where, }\ A(t)=\left.\frac{\partial f(\xi,t)}{\partial\xi}\right|_{\xi_0},\quad B_v=\begin{bmatrix}0&1&0&0\\0&0&0&1\end{bmatrix}^T\tag{14a}$$

$$B_\tau=I_4\ (=4\times4\ \text{identity matrix})\tag{14b}$$

$$v(t)=\begin{bmatrix}v_{F_Y}&v_{M_z}\end{bmatrix}^T\tag{14c}$$

$$\tau(t)=f(\xi_0,t)-A(t)\cdot\xi_0\tag{14d}$$

Here, we exclude the first two states (X,V_X) and the model is reduced to a 4-state system (Y,V_Y,ψ,r), because we are mainly concerned about the vehicle lateral displacement error and yaw directional motion. From Eq. (14), the numerical

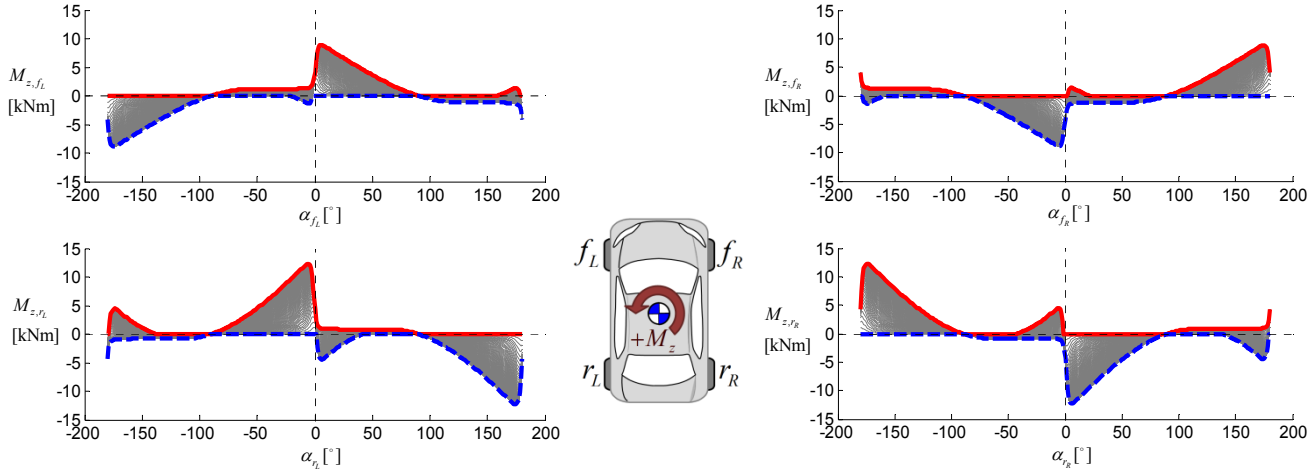

FIGURE 3. Vehicle yaw moments that can be generated by braking each wheel. The shaded area between red line (upper bound) and blue dotted line (lower bound) depicts achievable region for all possible slip ratio (-1≤λ≤0)

discretization is applied to build a time-varying linear, discrete time, state-space system with a sampling time (T_S):

$$\xi_{k+1} = A_{d,k} \cdot \xi_k + B_{v,d} \cdot v_k + B_{\tau,d} \cdot \tau_k \tag{15}$$

Here, we assume that the coefficients in the system and input matrices are constant over the horizon n:

$$\overline{A} \triangleq A_{d,k} \approx A_{d,k+1} \approx \cdots \approx A_{d,k+n-1} \tag{16}$$

$$\overline{B}_v \triangleq B_{v,d} \tag{17}$$

$$\overline{B}_\tau \triangleq B_{\tau,d} \tag{18}$$

$$\overline{\tau} \triangleq \tau_k \approx \tau_{k+1} \approx \cdots \approx \tau_{k+n-1} \tag{19}$$

The sequence of prediction state over the time horizon (n-steps) can be expanded as:

$$\begin{aligned}
\xi_{k+1} &= \overline{A}\xi_k + \overline{B}_v v_k + \overline{B}_\tau \overline{\tau} \\
\xi_{k+2} &= \overline{A}^2 \xi_k + \overline{A}\overline{B}_v v_k + \overline{B}_v v_{k+1} + \left(\overline{A}\overline{B}_\tau + \overline{B}_\tau\right)\overline{\tau} \\
&\vdots \\
\xi_{k+n} &= \overline{A}^n \xi_k + \overline{A}^{n-1}\overline{B}_v v_k + \overline{A}^{n-2}\overline{B}_v v_{k+1} + \ldots \\
&\quad + \overline{A}^2 \overline{B}_v v_{k+n-2} + \overline{A}\overline{B}_v v_{k+n-2} + \overline{B}_v v_{k+n-1} \\
&\quad + \left(\overline{A}^{n-1}\overline{B}_\tau + \overline{A}^{n-2}\overline{B}_\tau + \cdots + \overline{A}\overline{B}_\tau + \overline{B}_\tau\right)\overline{\tau}
\end{aligned} \tag{20}$$

Note that the states at a future moment are dependent on the current states and other sequence terms. This can be summarized with a matrix form:

$$\underset{\rightarrow n}{\Xi} = G_\xi \cdot \xi_k + H \cdot \underset{\rightarrow n-1}{V} + W \cdot T \tag{21}$$

where,

$$\underset{\rightarrow n}{\Xi} = \begin{bmatrix} \xi_{k+1} \\ \xi_{k+2} \\ \xi_{k+3} \\ \vdots \\ \xi_{k+n} \end{bmatrix},\ G_\xi = \begin{bmatrix} \overline{A} \\ \overline{A}^2 \\ \overline{A}^3 \\ \vdots \\ \overline{A}^n \end{bmatrix},\ \underset{\rightarrow n-1}{V} = \begin{bmatrix} v_k \\ v_{k+1} \\ v_{k+2} \\ \vdots \\ v_{k+n-1} \end{bmatrix},\ T = \begin{bmatrix} 1 \\ 1 \\ 1 \\ \vdots \\ 1 \end{bmatrix}\overline{\tau} \tag{21a}$$

$$H = \begin{bmatrix} \overline{B}_v & 0 & 0 & \cdots & 0 \\ \overline{A}\overline{B}_v & \overline{B}_v & 0 & \cdots & 0 \\ \overline{A}^2\overline{B}_v & \overline{A}\overline{B}_v & \overline{B}_v & \cdots & 0 \\ \vdots & \vdots & \vdots & \ddots & \vdots \\ \overline{A}^{n-1}\overline{B}_v & \overline{A}^{n-2}\overline{B}_v & \overline{A}^{n-3}\overline{B}_v & \cdots & \overline{B}_v \end{bmatrix} \tag{21b}$$

$$W = \begin{bmatrix} \overline{B}_\tau & 0 & 0 & \cdots & 0 \\ \overline{A}\overline{B}_\tau & \overline{B}_\tau & 0 & \cdots & 0 \\ \overline{A}^2\overline{B}_\tau & \overline{A}\overline{B}_\tau & \overline{B}_\tau & \cdots & 0 \\ \vdots & \vdots & \vdots & \ddots & \vdots \\ \overline{A}^{n-1}\overline{B}_\tau & \overline{A}^{n-2}\overline{B}_\tau & \overline{A}^{n-3}\overline{B}_\tau & \cdots & \overline{B}_\tau \end{bmatrix} \tag{21c}$$

Optimal Problem Formulation

The control goal is to minimize both the lateral deviation from the original course and to achieve a safe heading angle while minimizing control efforts. So, the cost function is defined as the summation of weighted state deviation and weighted control input sequence.

$$J = \sum_{i=1}^{n+1} \tilde{\xi}_{k+i}^T \cdot Q \cdot \tilde{\xi}_{k+i} + \sum_{i=0}^{n} v_{k+i}^T \cdot R \cdot v_{k+i} \tag{22}$$

where, Q and R are diagonal weighting matrices and the state deviations are $\tilde{\xi}_{k+i} = \xi_{k+i} - \xi_{k,desired}$. The desired state ($\xi_{k,desired}$) are predetermined by the offline optimal computation. In the present work, the structure of environment for the controlled vehicle is assumed to be known as straight road with multiple lanes. So the offline optimal calculation determines a safer heading angle (0°, 180°, 360°, etc.) which minimizes the lateral deviation under the given initial impact conditions.

Here, we set the same time horizon (n) for both predicted states and input sequences. But, once the optimal control set ($\underset{\rightarrow n-1}{V}^*$) is found, only the first control step (v_k^*) will be implemented. Then, Eq. (22) can be rewritten using a more compact notation as follows:

$$J = \underset{\rightarrow n}{\tilde{\Xi}}^T \cdot diag\left(Q\right) \cdot \underset{\rightarrow n}{\tilde{\Xi}} + \underset{\rightarrow n-1}{V}^T \cdot diag\left(R\right) \cdot \underset{\rightarrow n-1}{V} \tag{23}$$

where $diag\left(Q\right)$ and $diag\left(R\right)$ are block diagonal matrices.

By substituting Eq. (21), one can rearrange Eq. (23) so that the problem becomes a quadratic form of $\underset{\rightarrow n-1}{V}$:

$$\begin{aligned}
J = {} & \underset{\rightarrow n-1}{V}^T \left(H^T Q H + R\right) \underset{\rightarrow n-1}{V} + 2 \underset{\rightarrow n-1}{V}^T H^T Q \left(G_\xi \tilde{\xi}_k + WT\right) \\
& + \left(G_\xi \tilde{\xi}_k\right)^T Q \left(G_\xi \tilde{\xi}_k\right) + 2\left(WT\right)^T Q \left(G_\xi \tilde{\xi}_k\right) + \left(WT\right)^T Q \left(WT\right)
\end{aligned} \tag{24}$$

Since the last three terms in Eq. (24) are not affected by the input sequence ($\underset{\rightarrow n-1}{V}$), those terms can be ignored when figuring out the optimal input sequence to minimize J. This allows the control objective to be formulated in a simpler quadratic form:

$$\min_{\underset{\rightarrow n-1}{V}} J = \underset{\rightarrow n-1}{V}^T \cdot S \cdot \underset{\rightarrow n-1}{V} + 2 \cdot \underset{\rightarrow n-1}{V}^T \cdot f \tag{25}$$

$$\text{where,} \quad S = H^T Q H + R, \quad f = H^T Q \left(G_\xi \tilde{\xi}_k + WT\right) \tag{25a}$$

Constraints Handling

Constraints on the control magnitude and rate of change can be defined by the following inequality relationships:

$$\begin{bmatrix} v_k^{\min} \\ v_{k+1}^{\min} \\ \vdots \\ v_{k+n}^{\min} \end{bmatrix} \le \begin{bmatrix} v_k \\ v_{k+1} \\ \vdots \\ v_{k+n} \end{bmatrix} \le \begin{bmatrix} v_k^{\max} \\ v_{k+1}^{\max} \\ \vdots \\ v_{k+n}^{\max} \end{bmatrix} \tag{26}$$

$$\Delta v^{\min} \le v_{k+i} - v_{k+i-1} \le \Delta v^{\max} \tag{27}$$

Note that the control limits vary along the prediction horizon, as shown in Fig. 3. This is because the ranges between maximum and minimum virtual controls changes with tire slip angle and heading angle. In other words, the constraints are functions of the states and control inputs. After rearranging and combining Eqs. (26) and (27), one can obtain a simplified constraint expression based on the derivation in [18] as:

$$h\left(\underset{\to n}{\Xi}, \underset{\to n-1}{V}\right) < 0 \tag{28}$$

Then, we have a general quadratic programming problem with inequality constraints, which can be solved by using *MATLAB* Optimization Toolbox (*quadprog*).

$$\begin{aligned} &\min_{\underset{\to n-1}{V}} && J\left(\xi_k, \underset{\to n-1}{V}\right) \\ &\text{subject to} && h\left(\underset{\to n}{\Xi}, \underset{\to n-1}{V}\right) < 0 \end{aligned} \tag{29}$$

THE OPTIMAL ALLOCATION PROBLEM

The control laws derived in the previous section compute the optimal virtual controls. As shown in Fig. 4, the virtual control commands are fed to the wheel brake optimal allocation module to determine the effective physical controls. Since we assume that the real controls are the individual wheel brakes, the outputs of this module are the longitudinal wheel brake forces of each tire. Specifically, the objective of this module is to find optimal control $u_k^* \in \mathbb{R}^4$ to achieve the virtual control sequence $v_k^* \in \mathbb{R}^2$.

Tire Force Relationship

In Eq. (14), the relationship $g(\xi, u, t) = B_v \cdot v$ can be rewritten as:

$$g(\xi, u, t) = B_u \cdot u + W_d \cdot d \tag{30}$$

where, $d = \left[\Delta F_{y,f_L} \quad \Delta F_{y,f_R} \quad \Delta F_{y,r_L} \quad \Delta F_{y,r_R}\right]$

To replace the induced lateral force term d as a function of u, we utilize the force coupling effect. The tire forces are constrained by an enveloping curve, called a friction circle or friction ellipse [20]. The Magic Formula used in this research inherently describes combined forces within this friction ellipse, and this profile can be constructed as a linear function with manipulating tire model equations. From the definition in Eq. (5), one can analytically get the gradients of forces ($F_{x,\oplus_\odot}, F_{y,\oplus_\odot}$) with respect to λ ($= s_x$).

$$\frac{\partial F_{x,tire}}{\partial s_x} = \frac{F_p s_y^2}{\left(s_x^2 + s_y^2\right)^{3/2}} \cdot P\left(\frac{C_\alpha \|s\|}{F_p}\right) + P'\left(\frac{C_\alpha \|s\|}{F_p}\right) \cdot \frac{C_\alpha s_x^2}{s_x^2 + s_y^2} \tag{31}$$

$$\frac{\partial F_{y,tire}}{\partial s_x} = \frac{-F_p s_x s_y}{\left(s_x^2 + s_y^2\right)^{3/2}} \cdot P\left(\frac{C_\alpha \|s\|}{F_p}\right) + P'\left(\frac{C_\alpha \|s\|}{F_p}\right) \cdot \frac{C_\alpha s_x s_y}{s_x^2 + s_y^2} \tag{32}$$

$$\Gamma \triangleq \frac{\partial \Delta F_{y,tire}}{\partial F_{x,tire}} = \frac{\partial\left(F_{y,tire} - F_{y,tire}^0\right)}{\partial s_x} \cdot \frac{\partial s_x}{\partial F_{x,tire}} = \frac{\partial F_{y,tire}}{\partial s_x} \cdot \frac{\partial s_x}{\partial F_{x,tire}} \tag{33}$$

This matrix $\Gamma^{4\times 4}$ is a diagonal matrix which maps the tire longitudinal forces onto the lateral forces, $\Delta F_{y,\oplus_\odot} = \Gamma \cdot F_{x,\oplus_\odot}$

$$\Gamma = diag\left[\frac{\partial \Delta F_{y,f_L}}{\partial F_{x,f_L}} \quad \frac{\partial \Delta F_{y,f_R}}{\partial F_{x,f_R}} \quad \frac{\partial \Delta F_{y,r_L}}{\partial F_{x,r_L}} \quad \frac{\partial \Delta F_{y,r_R}}{\partial F_{x,r_R}}\right] \tag{34}$$

Then, Eq. (30) becomes:

$$B_v \cdot v = \left(B_u + W_d \cdot \Gamma\right) \cdot u \tag{35}$$

Solution of the Allocation Problem

The optimal allocation problem solves the linear relationship, Eq. (35), in the least-squares sense subject to the actuator saturation limit. Since the actuators are wheel brake forces, the control bounds are $F_{x,\oplus_\odot}^{\min} \le u \le F_{x,\oplus_\odot}^{\max}$. Because we consider a brake control action only, the value u should be negative. We employ the following least-squares problem for optimal allocation:

$$\min_{u_k}\left(\|u_k\|_2^2 + w \cdot \left\|\left(B_u + W_d \cdot \Gamma\right) \cdot u_k - B_v \cdot v_k^*\right\|_2^2\right) \tag{36}$$

$$\text{subject to} \qquad u^{\min}\left(\xi_k\right) \le u_k \le u^{\max}\left(\xi_k\right) \tag{37}$$

where the parameter w is a positive weighting factor chosen to achieve the relationship in (35) as close as possible.

SIMULATION RESULTS

The simulated scenario is that two vehicles are involved in a crash on a straight road. Then the collision leads the vehicle to travel into the opposite traffic lane if no control is applied. For this simulation, all state measurements such as position, speed, yaw rate, and heading angle are assumed to be available and accurate, and actuator delays are not included. In addition, all actuators are assumed to function normally. The vehicle used in the simulation is a big SUV defined in Carsim, the vehicle dynamics software ($m = 2450kg, I_z = 4946kgm^2$, $a = 1.105m$, $b = 1.7$). It is assumed that the vehicle is traveling straight with an initial longitudinal speed of 30m/s on a flat and straight road. The first impact is assumed to result in the initial conditions: lateral speed 5.0m/s, heading angle 9.2º, and yaw rate 114.6º/sec. The discrete time to run simulation is 0.01sec, and the sampling time for every linearization and the time horizon for MPC are set to 0.2 sec (20 steps).

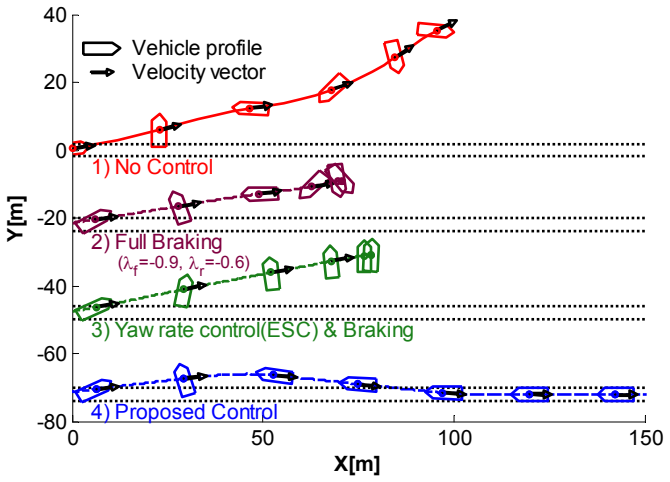

FIGURE 5. Vehicle trajectory comparison results for three control strategies. (Vehicle sizes are doubled.)

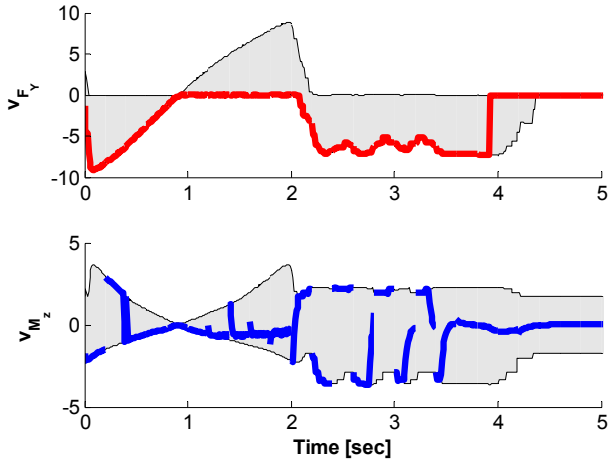

FIGURE 6. Virtual control inputs from the proposed control strategy. Feasible boundaries are shown by gray shaded regions between black lines. Virtual controls solved by MPC are shown with bold lines.

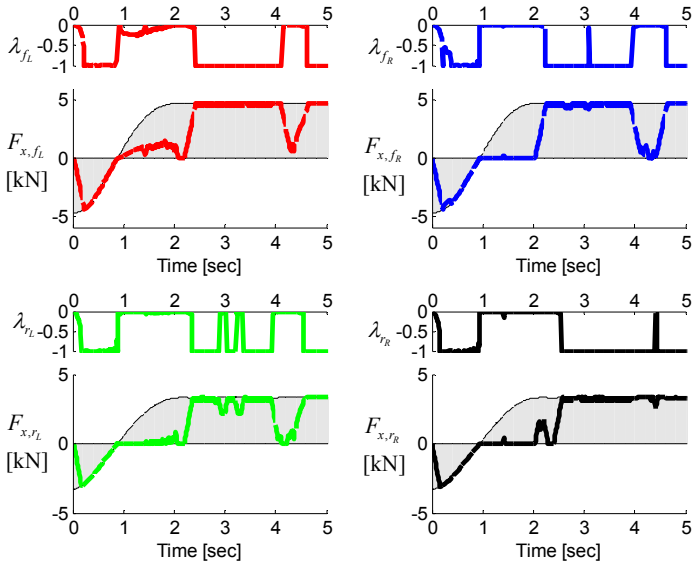

FIGURE 7. Longitudinal tire slip ratio commands and corresponding longitudinal tire forces calculated by the optimal allocation problem. The gray shaded regions depict feasible control bounds.

Weights on tracking error and input rates are Q= *diag*[1000 10 100 10] and R= *diag*[0.1 0.1]. Four vehicle trajectories with different control strategies are presented in Fig. 5 for comparison. It is shown that the vehicle with the proposed controller settles into a safe final heading angle of 180º and returns to the original lane. In contrast, the vehicles without braking intervention and with other control strategies depart from their original lane and can be broadsided by vehicles in other lanes. In the case of yaw rate control, the brake control actions to change the vehicle yaw motion are very limited at the

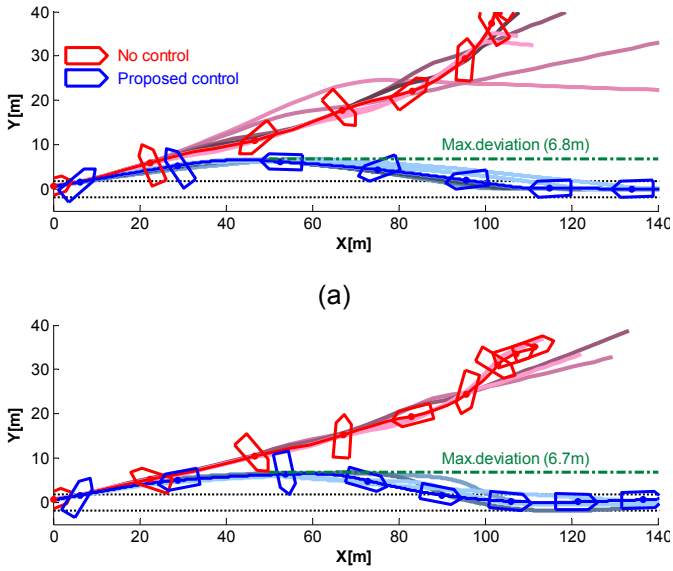

FIGURE 8. Vehicle trajectories under several initial conditions representing different levels of impact: (a) yaw rate 80~150°/s and heading angle 8~17° (b) yaw rate 160~200°/s and heading angle 18~23°, the initial lateral speed (5m/s) and longitudinal speed (30m/s) are the same.

end of the maneuver because the tire slip angles are all around ±90º, as analyzed in Fig. 3. Moreover, attempting to return the vehicle to the original lane (i.e. heading angle to the original 0º) can cause a large lateral deviation [21]. The virtual control bounds and control results from LTV-MPC are shown in Fig. 6. It should be noted that the feasible ranges vary with vehicle states; and the solution from MPC is reasonable only when considering these realistic constraint conditions. Although the constraints show a nonlinear nature, the quadratic programming is still applicable to solve the MPC problem through the system linearization process at every operation point. The results of optimal allocation are shown in Fig. 7. At the beginning of the control process, the brake control commands are determined to achieve a rapid yaw rotation. In this case, the rear wheel brake reactions are shown to have little faster responses than the front ones. This action makes it possible to pass by the region where the effectiveness of brake control (control authority) is little or none (around 1 second). After that, wheel commands are regulated to follow the yaw moment which leads the vehicle heading angle to the desired state, 180º.

In Fig. 8, the capability of the proposed control strategy is evaluated with several tests executed in different initial impact conditions. The simulated crash scenario has a similar layout to that of Fig. 5, but with different values for initial yaw rate and heading angle representing various levels of initial impacts. Overall, it is seen that the proposed control reduces the maximum lane deviations and brings the vehicle back to the original lane with the desired heading angle of 180º or 360º.

Although the 180º heading angle might be considered as a dangerous vehicle state by some, the situation is still safer than the case where the vehicle is exposed to a side impact from approaching traffic in the lanes other than the original lane.

CONCLUSIONS

This paper presents a LTV-MPC and optimal allocation algorithm to mitigate the secondary collision after an initial impact. These two optimization formulations exploit the feasible control bounds based on the physical constraints. From the proposed control system, wheel brake commands are determined so that the impact induced vehicle motion can be settled into a safe heading angle with a small lateral deviation. Simulations are performed for various initial conditions of yaw and lateral motion due to an impact. Simulation results show that the proposed control algorithm can effectively lead a vehicle to a desired heading angle with a smaller lateral deviation comparing to results from the uncontrolled case and other control strategies.

To enhance the control effectiveness, future work will add an active steering control to expand the control authority with changing side slip angles when brake controls are limited. The overall control objective can then be achieved by an integrated control strategy. Moreover, the practical performance of the designed scheme can be further studied by addressing the effect of driver's steering and braking action. A coordination or prioritization strategy between the control commands and the driver action needs to be considered.

REFERENCES

[1] NHTSA, "Traffic Safety Facts," US Department of Transportation 2012.

[2] J. Bahouth and K. Digges, "Characteristics of Multiple Impact Crashes That Produce Serious Injuries," in Proceedings of the 19th International Technical Conference on the Enhanced Safety of Vehicles, Washington DC, USA, 2005.

[3] U. Sander, K. Mroz, O. Boström, and R. Fredriksson, "The effect of pre-pretensioning in multiple impact crashes," in 21st International Technical Conference on the Enhanced Safety of Vehicles (ESV), 2009.

[4] A. Togawa, D. Murakami, H. Saeki, C. Pal, and T. Okabe, "An Insight into Multiple Impact Crash Statistics to Search for Future Directions of Counter-Approaches," in 22th International Technical Conference on the Enhanced Safety of Vehicles (ESV), 2011.

[5] J. Zhou, "Active Safety Measures for Vehicles Involved in Light Vehicle-to-Vehicle Impacts," Ph.D. Thesis, The University of Michigan, Ann Arbor, MI, 2009.

[6] T. Ayres, L. Li, D. Trachtman, and D. Young, "Passenger-side rear-view mirrors: driver behavior and safety," International journal of industrial ergonomics, vol. 35, pp. 157-162, 2005.

[7] A. Eigen and W. Najm, "Problem definition for pre-crash sensing advanced restraints," DOT HS 811 114, 2009.

[8] J. Lenard and R. Frampton, "Two-Impact Crashes-Implications for Occupant Protection Technologies," in Proceedings of 18th International Technical Conference on the Enhanced Safety of Vehicles, Nagoya, Japan, 2003.

[9] B. Fildes, J. C. Lane, J. Lenard, and A. Vulcan, "Passenger cars and occupant injury: side impact crashes," 1994.

[10] D. Yang, B. Jacobson, and M. Lidberg, "Benefit prediction of passenger car post impact stability control based on accident statistics and vehicle dynamics simulations," in Proceedings of 21st IAVSD Symposium on Dynamics of Vehicles on Roads and Tracks, 2009.

[11] S. A. Ferguson, "The effectiveness of electronic stability control in reducing real-world crashes: a literature review," Traffic Injury Prevention, vol. 8, pp. 329-338, 2007.

[12] C. Chan, and H. Tan, "Feasibility Analysis of Steering Control as a Driver-Assistance Function in Collision Situations," IEEE Trans. On Intelligent Transportation Systems, pp. 1–9, 2001.

[13] D. Yang, T. Gordon, et al., "Post-Impact Vehicle Path Control by Optimization of Individual Wheel Braking Sequences," Proc. of 10th International Symposium on AVEC 2010, pp. 882-887

[14] J. Zhou, J. Lu, and H. Peng, "Vehicle stabilization in response to exogenous impulsive disturbances to the vehicle body," In Proc. of the American Control Conference, St. Louis, MO, pp. 701-706, 2009.

[15] EURO-NCAP. (2012). Audi Secondary Collision Brake Assist. Available: http://www.euroncap.com/rewards/audi_secondary_collision_brake_assist.aspx

[16] J. Yoon, H. Peng, "Sideslip Angle Estimation Based on GPS and Magnetometer Measurements," Proc. 11th International Symposium on AVEC, Seoul, Korea, 2012.

[17] H. Pacejka, Tire and Vehicle Dynamics (Second edition), SAE International, 2005.

[18] J. Maciejowski, Predictive Control with Constraints. Prentice-Hall, London

[19] P. Falcone, F. Borrelli, J. Asgari, H. Tseng, and D. Hrovat, "Predictive active steering control for autonomous vehicle systems," IEEE Trans. Contr. Systems Technology, vol. 15, no. 3, pp. 566–580, 2007.

[20] J. Wong, Theory of Ground Vehicles, 3rd Edition. John Wiley & Sons, 2001.

[21] J. Zhou, J. Lu, and H. Peng, "Vehicle Dynamics in Response to the Maneuver of Precision Immobilization Technique," In Proc. of ASME Dynamic Systems and Control Conference, Ann Arbor, MI, 2008.